ISIJ International, Vol. 39 (1999), No. 5, pp. 426–434

Agglomeration and Flotation of Alumina Clusters in Molten Steel

Hirokazu TOZAWA, Yoshiei KATO,[1] Kenichi SORIMACHI[2] and Tomomi NAKANISHI[3]

Formerly Technical Research Laboratories, Kawasaki Steel Corp.. Now at Technology Group on the Environment-friendly Steelmaking Processes, The Japan Research and Development Center for Metals, Toranomon, Minato-ku, Tokyo, 105-0001 Japan. 1) Technical Research Laboratories, Kawasaki Steel Corp., Kawasaki-dori, Mizushima, Kurashiki, Okayama-ken, 712-8511 Japan. 2) Technical Research Laboratories, Kawasaki Steel Corp., Kawasaki-cho, Chuo-ku, Chiba, Chiba-ken, 260-0835 Japan. 3) Nishi-nihon District Office, Kawasaki Steel System R & D Corp., Kawasaki-dori, Mizushima, Kurashiki, Okayama-ken, 712-8511 Japan.

(Received on August 24, 1998; accepted in final form on February 9, 1999)

An equation for the floating velocity of cluster-shaped alumina inclusions which considers changes in average density was derived by quantifying the size and density of alumina clusters using fractal theory. The results obtained showed that the dependency of the floating velocity on the cluster diameter is smaller than in the conventional equations, which assume that clusters have a uniform average density. In particular, the floating velocity of clusters 100 μm and over is considerably smaller than the conventional floating velocity.

A model of the coalescence of cluster-shaped inclusions was also constructed, and the behavior of alumina clusters in molten steel in the tundish of an actual continuous casting machine was analyzed considering floating characteristics and agglomeration. The calculated results showed good agreement with the results measured in the actual machine, demonstrating that it is possible to simulate the coalescence and floating separation of cluster inclusions in molten steel with this model.

KEY WORDS: cluster; fractal dimension; alumina; agglomeration; floating velocity; modelling; simulation; inclusion; tundish; steelmaking.

1. Introduction

When molten steel is deoxidized with aluminum, small particles of alumina collect in relatively loose, irregularly-shaped groups to form so-called alumina clusters, which can cause defects in cold-rolled sheets and other steel materials if some of these inclusions remain at the surface or interior of continuously cast slabs. Complete separation and removal of inclusions in the steelmaking process are therefore essential. An effective means of removing inclusions is to promote collision and coalescence of the inclusion particles by stirring the molten steel and float out and separate the inclusions by coarsening.

Basic research on the removal of inclusions includes an inclusion separation model proposed by Lindborg and Torssel,[1] in which coarsening of the inclusions due to Stokes and gradient collisions is the rate governing process, and a general model proposed by Linder,[2] which considers the turbulent collision of deoxidation products, material adhering to the vessel wall, and floating separation. Nakanishi and Szekely[3] analyzed the rate of Al deoxidation of molten steel in an ASEA-SKF furnace based on turbulent cohesion theory and the results of a flow simulation, Shirabe and Szekely[4] analyzed the turbulent coalescence of deoxidation products in an RH degasser and calculated the particle concentration distribution and particle size distribution.

The calculations mentioned above assume that inclusions are spherical particles which agglomerate to form spherical particles with a larger particle diameter. However, it is conceivable that small particles such as alumina-type inclusions exhibit a different behavior when they collect in a cluster morphology in molten steel.[5,6] Moreover, although the floating characteristics of spherical inclusions can be expressed by Stokes' law in the field of fluid dynamics,[7] the floating behavior of cluster-shaped inclusions has not necessarily been clarified.

Therefore, in this research, the size and density of alumina clusters were quantified using fractal theory, which has rarely been adopted in steelmaking research to date, and the floating characteristics of the clusters were clarified by model experiments. A model of the coalescence of cluster-shaped inclusions by Brownian coagulation, turbulent coagulation, and differential coagulation was then constructed, and the behavior of alumina clusters in the molten steel in the tundish of an actual continuous casting machine was analyzed considering the above-mentioned floating characteristics and agglomeration.

2. Theoretical Analysis

2.1. Model of Collision and Coalescence of Alumina-type Inclusions

2.1.1. Fractal Dimension of Clusters

In the continuous casting of low carbon aluminum-

killed steel, more than 70% of the inclusions in the molten steel in the ladle before the metal is poured into the caster tundish and in the tundish itself are alumina clusters, which are formed when small particles of alumina collect in a cloud-like body.[6] Using fractal theory, the size of such alumina clusters and the distribution in three-dimensional space of the small particles which make up the clusters can be expressed quantitatively by Eq. (1)[8]:

$$N=\rho_n(R/r)^{Df} \quad \text{.....(1)}$$

Here, R is the size of the cluster (representative radius) (m), N is the number of constituent particles (—), r is the radius of the small particles which make up the cluster (m), Df is the fractal dimension of the cluster (—), and ρ_n is the numerical density. Because it is assumed that all the small particles have the same mass, N can be interpreted as the mass of the cluster, and ρ_n as the mass density.

Because the proportion of space which the cluster occupies can be characterized quantitatively by Df, it is possible to obtain the representative diameter of the cluster from Eq. (1) if the number of constituent particles is known.

2.1.2. Model of Cluster Collision and Coalescence

The main assumptions adopted in constructing a model of the collision and coalescence of alumina clusters were as follows.

1) The alumina cluster consists of a collection of N small spherical particles having a uniform radius r.
2) The size of the cluster (representative radius), R, is in accordance with Eq. (1), and the volume of the cluster, V, is equal to the volume of a sphere with the representative radius R.
3) In new clusters which are formed by the collision and coalescence of two clusters, the number of constituent particles is equal to the sum of the number of constituent particles in the two clusters, and the size of the new cluster is specified by the relationship in Eq. (1).
4) The frequency of collisions between alumina clusters is in accordance with the theory of the collision and coalescence of spherical particles.

According to the theory of the collision and coalescence of spherical particles, the frequency of collision, N_{ij}, per unit of time and unit of volume between two particles having the particle volumes v_i and v_j can be expressed by the following equation.[1,9]

$$N_{ij}=\beta(v_i, v_j)n_in_j \quad \text{.....(2)}$$

Here, $\beta(v_i, v_j)$ is a function of the frequency of collision between the two particles i and j (m^3/s), and is determined by the mode of flow and the size of the particles. Further, n_i and n_j are the numerical concentration of individual particles in i and j ($1/m^3$).

It is known that the agglomeration of inclusions in steel in the tundish progresses mainly by coagulation due to Brownian motion, coagulation due to differences in the floating velocity of inclusions, cohesion due to turbulent flows, and similar factors. The collision frequency functions for these respective coagulation mechanisms may be introduced as follows.

Brownian coagulation[10]:

$$\beta_b(v_i,v_j)=\frac{2kT}{3\mu}\left(\frac{1}{v_i^{1/3}}+\frac{1}{v_j^{1/3}}\right)(v_i^{1/3}+v_j^{1/3}) \quad \text{.....(3)}$$

Differential coagulation[1,9]:

$$\beta_d(v_i, v_j)=\pi(a_i-a_j)^2|v_i-v_j| \quad \text{.....(4)}$$

Turbulent coagulation[11]:

$$\beta_t(v_i, v_j)=\alpha_T 1.3(a_i+a_j)^3\left(\frac{\varepsilon}{\nu}\right)^{1/2} \quad \text{.....(5)}$$

Accordingly, the collision frequency function for inclusions in steel in the tundish can be expressed by Eq. (6).

$$\beta(v_i, v_j)=\beta_b(v_i, v_j)+\beta_d(v_i, v_j)+\beta_t(v_i, v_j) \quad \text{.....(6)}$$

Here, v_i, v_j are the volume of the particles (m^3), k is Boltzmann constant (J/K), T is the absolute temperature (K), μ is the viscosity of the fluid (Pa·s), a_i, a_j are the radii of the spherical particles (m), v_i, v_j are the floating velocities of the particles (m/s), ν is the kinematic viscosity of the fluid (m^2/s), ε is the dissipation rate of turbulent kinetic energy (m^2/s^3), and α_T is coagulation coefficient (—).

Equation (5) was derived by Higashitani *et al.*[11] by considering coagulation coefficient due to the hydrodynamic interaction and dispersion force in an equation proposed by Saffman and Turner.[12] The coagulation coefficient in the equation is graphed against a non-dimensional number N_T ($=6\pi\mu a^3\dot{\gamma}/A$) which includes Hamaker's constant A(J) ($=0.45\times10^{-20}$ J)[9] and a deformation rate $\dot{\gamma}$ ($=(4\varepsilon/15\pi\nu)^{0.5}$) (1/s), and can be expressed by the following equation.

$$\log\alpha_T=-0.24\log N_T+0.047 \quad \text{.....(7)}$$

In the case of cluster-shaped inclusions, these equations are applied in the same manner by substituting the representative radius, R, and volume, V, of the alumina clusters for the radius, a, and volume, v, in Eqs. (2) through (7).

When a cluster-shaped inclusion consisting of i constituent particles (hereinafter referred to as an inclusion with a clustering degree of i) and an inclusion with a clustering degree of j collide and coalesce, the rate of change in concentration of an inclusion with a clustering degree of k ($=i+j$) can be obtained if Eqs. (2) through (7) are substituted in the population balance equation in Eq. (8), which was derived by Smoluchowski.[10]

$$\frac{dn_k}{dt}=\frac{1}{2}\sum_{i+j=k}N_{ij}-\sum_{i=1}^{\infty}N_{ik}$$

$$=\frac{1}{2}\sum_{i+j=k}\beta(v_i, v_j)n_in_j-n_k\sum_{i=1}^{\infty}\beta(v_i, v_k)n_i \quad \text{....(8)}$$

The mass concentration c_i (mass%) of an inclusion with a clustering degree of i can be expressed approximately using the density of alumina, $\rho_{Al_2O_3}$ (kg/m^3), and the density of molten steel, ρ (kg/m^3), as follows:

$$c_i = i\frac{4\pi r^3}{3}\rho_{Al_2O_3} n_i/\rho \times 100 \quad \text{.....(9)}$$

Therefore, the rate of change in mass concentration of clusters $f(c_k)$ expressed in terms of weight concentration can be found by using the following equation, from Eqs. (8) and (9).

$$f(c_k) = \frac{Ck}{r^3}\left(\frac{1}{2}\sum_{i+j=k}\beta(v_i, v_j)\frac{c_i}{i}\frac{c_j}{j} - \frac{c_k}{k}\sum_{i=1}^{\infty}\beta(v_i, v_k)\frac{c_i}{i}\right) \quad \text{.....(10)}$$

Here, $C = 3\rho/(4\pi\rho_{Al_2O_3}) \times 10^{-4} = 4.248 \times 10^{-5}$.

2.2. Basic Equation of Flow Field

The main assumptions and the master equation for analysis of the agglomeration behavior of cluster-shaped inclusions in molten steel are presented below.

1) The k–ε model[13] is used for the turbulent flow model.
2) The concentration of inclusions is classified separately for each inclusion with a clustering degree of i.
3) The effective Schmidt number and the effective Prandtl number are equal to 1.
4) The terminal velocity of an inclusion is decided by its clustering degree, and has the same value for all inclusions with the same clustering degree.

Continuity equation:

$$\frac{\partial\rho}{\partial t} + \frac{\partial(\rho u_i)}{\partial x_i} = 0 \quad \text{.....(11)}$$

Momentum balance equation (considering temperature dependency):

$$\frac{\partial\rho}{\partial t} + \frac{\partial(\rho u_i u_j)}{\partial x_j} = -\frac{\partial p}{\partial x_i} + \frac{\partial}{\partial x_j}\left[\mu_{\text{eff}}\left(\frac{\partial u_i}{\partial x_j} + \frac{\partial u_j}{\partial x_i}\right)\right] + g_i(\rho - \rho_0) \quad \text{.....(12)}$$

Enthalpy balance equation:

$$\frac{\partial(\rho T)}{\partial t} + \frac{\partial(\rho u_i T)}{\partial x_i} = \frac{\partial}{\partial x_i}\left(\rho k_{\text{eff}}\frac{\partial T}{\partial x_i}\right) \quad \text{.....(13)}$$

The concentration equation for an inclusion with a clustering degree of i can be expressed as follows:

$$\frac{\partial(\rho c_i)}{\partial t} + \frac{\partial(\rho u_{ij}^* c_i)}{\partial x_j} = \frac{\partial}{\partial x_j}\left(\rho D_{\text{eff}}\frac{\partial c_i}{\partial x_j}\right) + \rho f(c_i) \quad i = 1 \text{ to } i_{\max} \quad \text{.....(14)}$$

Here, the following equation is introduced based on the above-mentioned assumption 3).

$$\rho k_{\text{eff}} = \rho D_{\text{eff}} = \mu_{\text{eff}} \quad \text{.....(15)}$$

The second term from the right in Eq. (14) is the term for formation by agglomeration, and therefore can be found using Eq. (10), in other words, as shown in Eq. (16). However, if the clustering degree after coalescence exceeds the set maximum clustering degree, $i_{\max}$, for reasons relating to the calculation procedure, Eq. (17) is used rather than Eq. (16).

Table 1. Geometry of Mizushima No. 4CC tundish and computational conditions.

Geometry	Length: 3.85m (half tundish) Width: 1.79m (max.), 0.65m (min.) Depth: 1.0m (max.)
Mass of steel melt	70, 000 kg
Throughput per strand	68.3 kg/s (4.1t/min)
[O] at inflow	50 ppm
Density of molten steel	$\rho = 7100 - 1.12(1560 - T)$ (ρ: kg/m^3, T: ℃)
Clustering degree (Number of particles in cluster)	i = 1 - 29

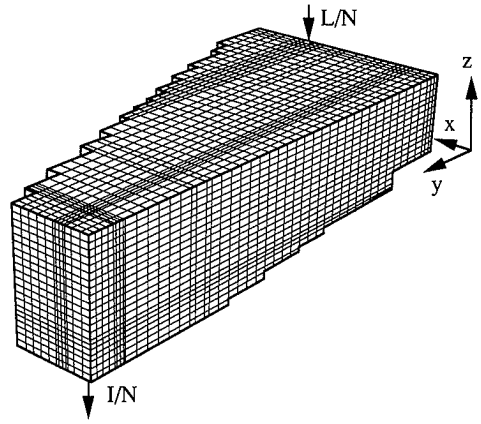

Fig. 1. Computational mesh (26 × 46 × 20 grid cells) and perspective view of half tundish.

$$f(c_i) = \frac{Ci}{r^3}\left(\frac{1}{2}\sum_{j+k=i}\beta(v_j, v_k)\frac{c_j}{j}\frac{c_k}{k} - \frac{c_i}{i}\sum_{j=1}^{i_{\max}}\beta(v_j, v_i)\frac{c_j}{j}\right) \quad i = 1 \text{ to } i_{\max} - 1 \quad \text{.....(16)}$$

$$f(c_i) = \frac{Ci}{r^3}\frac{1}{2}\sum_{j+k\geq i_{\max}}\beta(v_j, v_k)\frac{c_j}{j}\frac{c_k}{k} \quad i = i_{\max} \quad \text{..(17)}$$

Here, $u = (u_1, u_2, u_3)$ is the flow velocity vector of the molten steel (m/s), $\mu_{\text{eff}} = \mu + \mu_t$ is the effective viscosity of the molten steel (Pa·s), μ_t is the turbulent viscosity (Pa·s), p is pressure (Pa), T is temperature (K), g is acceleration due to gravity ($=9.8\,\text{m/s}^2$), ρ_0 is the density of steel at the standard temperature (kg/m^3), $u_i^* = (u_1, u_2, u_3 + v_i)$ is the flow velocity of an inclusion with a clustering degree of i (m/s), and v_i is the terminal floating velocity of the same inclusion (m/s).

2.3. Calculation and Boundary Conditions

Momentum, heat, and the mass balance of an inclusion with a clustering degree of i were solved in a coupled manner using the general-purpose code PHOENICS for fluid analysis by the calculus of finite differences. The object of this calculation was the tundish at No. 4 continuous casting machine at Kawasaki Steel Corporation's Mizushima Works. The conditions of the calculation are shown in **Table 1**. Assuming the symmetry of the tundish, the calculations were made using a 1/2 model. As shown in **Fig.1**, (the transverse direction x × the longitudinal direction y × the height of the tundish z) was divided into 26 × 46 × 20 elements. The cluster-

Table 2. Boundary conditions.

Wall boundaries	Standard wall conditions No-flux condition for alumina clusters Heat flux: $q_w = 5.24$ kcal / m^{2}s
Free surface	Frictionless impervious boundary Inclusion concentration: $q = 0.8\ v_i c_i$ Heat flux: $q_s = 11.27$ kcal / m^{2}s

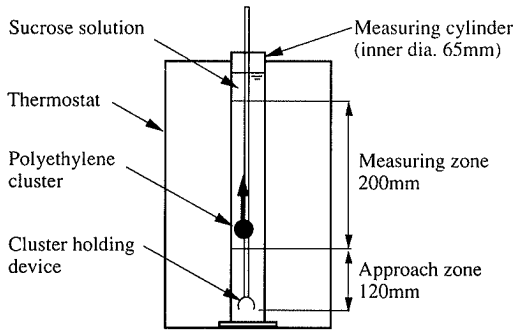

Fig. 2. Schematic diagram of experimental apparatus.

ing degree of inclusions was varied between 1 and 29.

The boundary conditions are shown in **Table 2**. Because it is considered that alumina inclusions do not adhere to the wall and that part of the inclusions which reach the free surface are again entrained in the molten steel, it was assumed here as fitting parameter of calculation that 80% of the inclusion flux, $v_i c_i$, which reaches the surface of the molten steel is removed, and the remaining 20% remains in the molten steel. For the heat flux from the walls and the free surface, measured values were used.

Assuming the density distribution, n_i^0, of the initial number of inclusions with a clustering degree of i in the molten steel which flows from the ladle through the pouring pipe can be expressed in the form of an index function of the representative radius, R_i, of the inclusions,

$$n_i^0 = N_0 \exp(-\alpha_1 R_i) \quad \text{.....(18)}$$

The initial mass concentration distribution, c_i^0 (mass%), can be expressed by the following equation by substituting the Eq. (18) into Eq. (9).

$$c_i^0 = i\frac{4\pi r^3}{3} \rho_{Al_2O_3} N_0 \exp(-\alpha_1 R_i)/\rho \times 100 \quad \text{....(19)}$$

Here, α_1, N_0 are constants, and α_1 was set at 3.45×10^5 (1/m) from the measured value at the tundish inlet hole. Further, N_0 is set so that the total calculated oxygen concentration in the alumina inclusions of each clustering degree is equal to the oxygen concentration of the molten steel.

3. Experimental Procedure

3.1. Cluster Floating Experiment Using Cold Model

The experimental apparatus is shown in **Fig. 2**. The measuring cylinder was filled with a sucrose solution, and the solution temperature was kept constant by surrounding the cylinder with a thermostat. The cluster

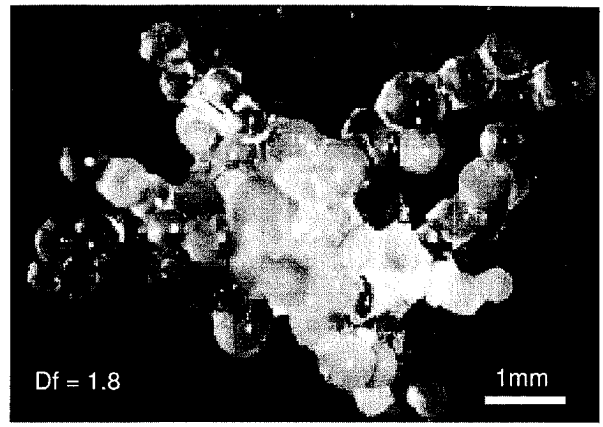

Fig. 3. Example of polyethylene cluster used in cold model experiment.

was immersed in the solution using a rotating-type cluster holding device, and kept for an adequate time to allow all air bubbles to escape from the cluster. Next, the holder was gently opened, and the cluster was allowed to float up from the bottom of the measuring cylinder. An approach zone was set to ensure that the floating velocity would reach the terminal velocity. The time required for floating was measured in the measuring zone above the approach zone, and the floating velocity of the cluster, v, was then calculated. The concentration of the sucrose solution was varied between 40 and 60 mass%, while the temperature was varied between 8.4 and 27.2°C (giving a density range of 1.17 to 1. 29 g/cm^3).

For this experiment, polyethylene clusters were made from spherical polyethylene particles (Flow Beads manufactured by Sumitomo Seika Co.) with a diameter of $600 \pm 100\ \mu$m and a density of 0.918 g/cm^3 by combining 10–100 particles into a cluster shape with an adhesive (specific gravity after drying, 1.189). The fractal dimension, Df, of these clusters was adjusted to 1.8. An example of a polyethylene cluster is shown in **Fig. 3**.

3.2. Measurement of Distribution of Alumina Clusters at Actual Continuous Casting Machine

No. 4 continuous casting machine at Kawasaki Steel's Mizushima Works has a throughput of 4.1 t/min per strand. During the casting of ultra-low carbon steel, molten steel is sampled from the vicinity of the pouring pipe (depth 400 mm) in the tundish and from the straight part of the immersion nozzle (depth 560 mm). The samples taken are measured to determine the oxygen content, and after grinding, a surface area approximately 800 mm^2 is observed at 400× magnification with an optical microscope. When two or more alumina particles with a size of approximately 0.5 μm or more are found in proximity, the particles are judged to be a cluster. Using a photograph, the number of constituent particles is counted, and the diameter of a circle circumscribed around the particles is measured as the diameter of the alumina cluster. The mass concentration is calculated from Eq. (9) using a constituent particle diameter of 3 μm, after converting the number of clusters per cross-sectional surface area to a number in the volume using DeHoff's equation.[14]

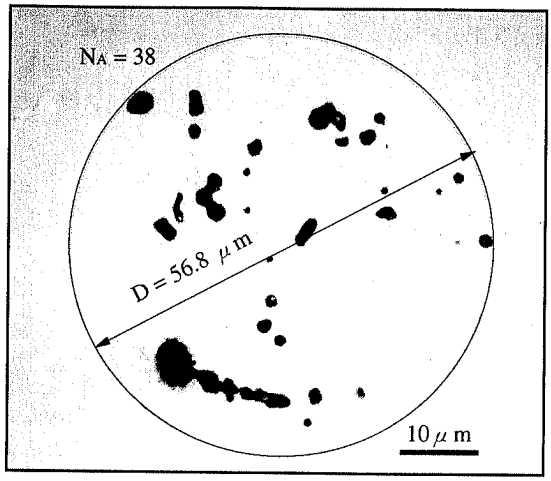

Fig. 4. Example of alumina cluster sampled from molten steel in ladle immediately before teeming into tundish.

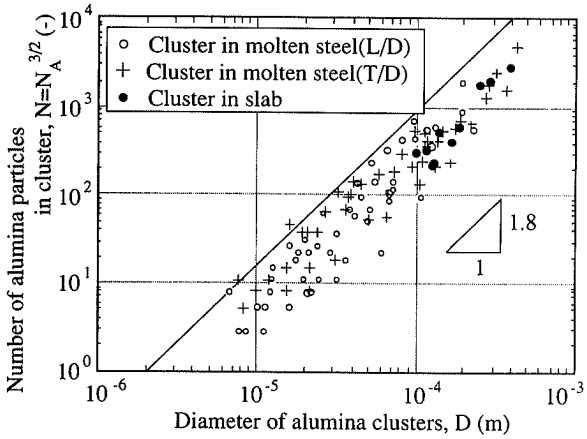

Fig. 5. Relationship between number of alumina particles and diameter of alumina clusters.

4. Results and Discussion

4.1. Cluster Distribution and Floating Characteristics

4.1.1. Fractal Dimension of Alumina Clusters

Figure 4 shows an example of an alumina cluster which was detected in a sample of molten steel in the ladle. **Figure 5** shows the relationship between the diameter, D, of alumina clusters and the number of particles, N, in the alumina clusters in samples taken from the ladle, tundish, and continuously cast slabs. The number of particles, N, was converted from N_A, which was measured on a 2-dimensional plane, to the number of particles in a 3-dimensional sphere using $N=N_A^{3/2}$. The N_A is largest when a cutting plane passes through in the vicinity of the center of gravity of clusters. In this case, the diameter D_A, which was measured on a 2-dimensional plane, is approximately equivalent to the diameter, D, of alumina clusters on a 3-dimension. From the relationship between upper limit of the N and D illustrated in Fig. 5, N can be expressed as:

$$N=\alpha D^{1.8} \quad \text{.....(20)}$$

Here, α is the proportional constant, and from the function $D=d$, when $N=1$, $\alpha=d^{-1.8}$. From this, it was found that the fractal dimension of the actual alumina clusters is 1.8.

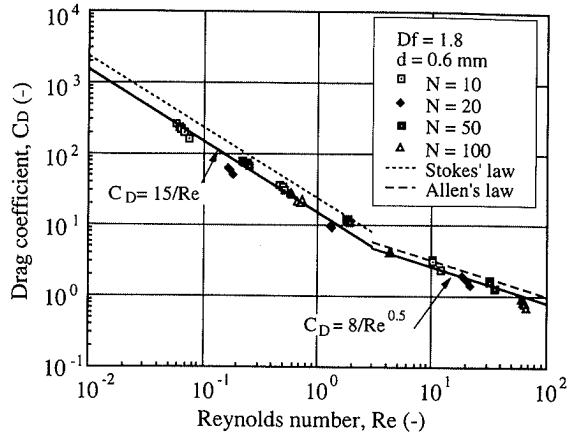

Fig. 6. Relationship between drag coefficient of polyethylene clusters and Reynolds number.

On the other hand, the fractal dimension of the general clusters which have been observed to date can be obtained using a computer simulation by random walk. According to a C1C1 (kinetic clustering of clusters) model for 3-dimension, Df is reported to be 1.78 ± 0.05.[15] Although the fractal dimension of alumina clusters has not previously been measured, the value found in the present work, 1.8, was substantially the same as this simulated result, and it was therefore concluded that the fractal value of alumina inclusions conforms to the fractal dimension of clusters in general.

4.1.2. Floating Characteristics of Clusters

Figure 6 shows the relationship between the drag coefficient, C_D, obtained from the floating velocity of the polyethylene clusters, and the Reynolds number, Re, which uses the cluster diameter, D, as the representative length. The following relations can be obtained, for clusters of 10 clustering degrees and over, using a value on the order of $Re=3$ as a transition.

$$C_D=15/Re \quad Re\leqq 3 \quad \text{.....(21)}$$

$$C_D=8/Re^{0.5} \quad 3<Re<100 \quad \text{.....(22)}$$

These values, as shown in Fig. 6, are small compared with the values for spheres obtained with Stokes' law ($C_D=24/Re$) and Allen's law ($C_D=10/Re^{0.5}$). This is an influence of the character of clusters that the number density of the constituent particles in a cluster is small toward the outer side. The branches made by constituent particles which extend as far as the circumference make virtually no contribution to drag.

An equilibrium Eq. (23) for buoyancy and drag can be introduced for clusters floating at a uniform velocity:

$$N\frac{\pi d^3}{6}(\rho-\rho_p)g=C_D\frac{\pi D^2}{4}\frac{\rho v^2}{2} \quad \text{.....(23)}$$

From Eq. (20) through (23), the floating velocity, v, can be expressed as follows for clusters of 10 clustering degrees and over.

$$v=\frac{8}{5}\frac{D^{0.8}d^{1.2}(\rho-\rho_p)g}{18\mu} \quad Re\leqq 3 \quad \text{.....(24)}$$

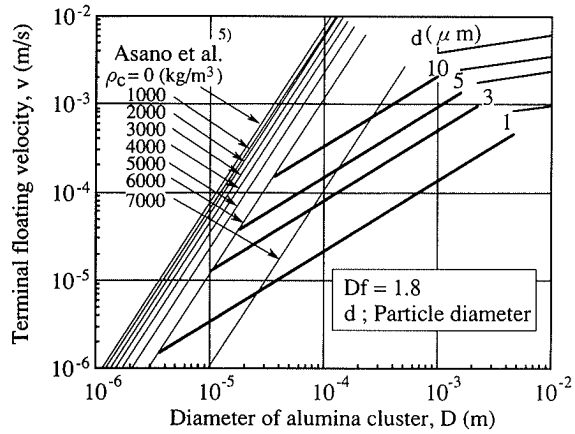

Fig. 7. Relationship between calculated terminal floating velocity in molten steel and diameter of alumina clusters.

$$v=\frac{D^{0.2}d^{0.8}(\rho-\rho_p)^{2/3}g^{2/3}}{6^{2/3}\rho^{1/3}\mu^{1/3}} \quad 3<Re<100 \quad ....(25)$$

Here, v is the floating velocity (m/s), D is the diameter of the cluster ($=2R$) (m), N is the number of constituent particles in the cluster (—), d is the diameter of the constituent particles (m), ρ_p is the density of the constituent particles (kg/m^3), C_D is the drag coefficient (—), ρ is the density of the fluid (kg/m^3), and μ is the viscosity of the fluid (Pa·s).

The terminal floating velocity of alumina clusters of 10 clustering degrees and over, in static molten steel, as calculated using Eqs. (24) and (25), is shown in **Fig. 7**. Though Eqs. (24) and (25) are derived from experiment data of 10 clustering degrees and over, the floating velocity, v of 2 clustering degrees calculated by Eq. (24) is over estimated around from 38 to 56%, it depends on the direction of the cluster, than the floating velocity calculated from analytical solution of two spheres.[16]

The floating velocity of the clusters increases as the cluster diameter and the diameters of the constituent particles increase. However, the dependency of the floating velocity on the cluster diameter is smaller in the present case than in the results obtained by Asano *et al.*,[5] who assumed that clusters have a uniform average density. This is because the average density of clusters, ρ_c, converges on the density of the molten steel as the cluster diameter increases, as shown by Eqs. (26) and (27).

$$\rho_c=\rho\varepsilon+\rho_{Al_2O_3}(1-\varepsilon) \quad .....(26)$$

$$\varepsilon=1-(d/D)^{3-Df} \quad .....(27)$$

Here, ρ_c is the average density of an alumina cluster (kg/m^3), ρ is the density of molten steel ($=7\,100$ kg/m^3), $\rho_{Al_2O_3}$ is the density of alumina ($=3\,990$ kg/m^3), ε is the volumetric fraction ratio of molten steel contained within the alumina cluster (—), d is the diameter of the constituent alumina particles (m), D is the diameter of the alumina cluster (m), and Df is the fractal dimension of the alumina cluster ($=1.8$).

The relationship between the volumetric fraction ratio of the alumina in an alumina cluster, $1-\varepsilon$, and the diameter of the alumina cluster is shown in **Fig. 8**. Although Asano *et al.*[5] reported a measured value of

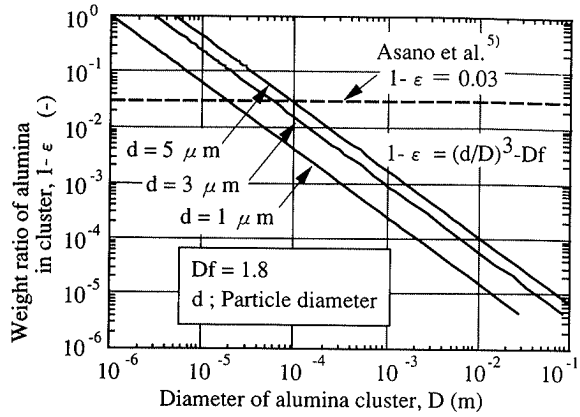

Fig. 8. Relation between $(1-\varepsilon)$ and diameter of alumina cluster.

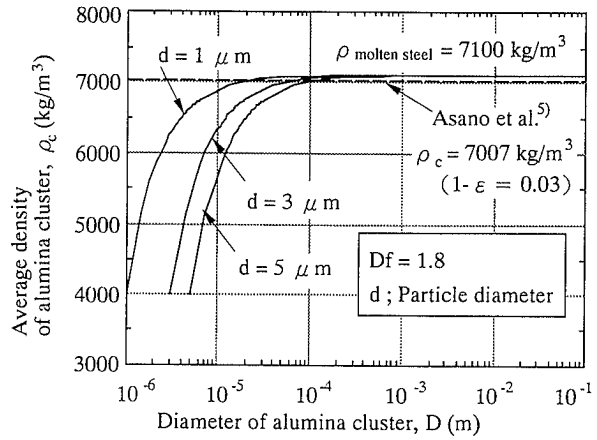

Fig. 9. Relationship between average density of alumina cluster in molten steel and diameter of alumina clusters.

0.03 for $1-\varepsilon$, this value becomes smaller than 0.03 in clusters with diameters of 100 μm and larger. The relationship between the average density and diameter of alumina clusters is shown in **Fig. 9**. In the case of Asano *et al.*, because 0.03 is used as the value of $1-\varepsilon$, the average density is constant at 7 007 kg/m^3 for all diameters. However, in the present research, in particular, the clusters of 1 mm and larger which are observed occasionally in steel slabs showed a value of $1-\varepsilon$ of 0.001 or under, and the average density of the alumina clusters was more than 99.9% that of molten steel. These differences result in a large difference in the evaluation of the floating velocity, as can be seen in Fig. 7.

4.2. Behavior of Alumina Clusters in Molten Steel

4.2.1. Flow Pattern, Concentration Distribution of Inclusions

Figure 10 shows an example of the computed velocity profile of molten steel in the tundish of an actual continuous casting machine with a molten steel capacity of 70 t and a throughput of 4.1 t/min per strand. The fluid which is discharged from the pouring pipe travels to the bottom with virtually no spreading. After impact against the bottom, the fluid flows along the bottom and then forms an upward current. The upward current divides, with one part becoming a circulating current between the upward current and the pouring flow, and

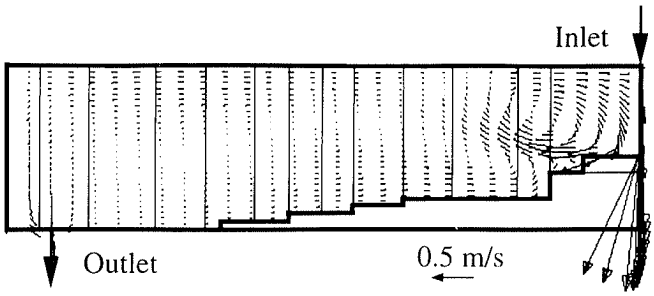

Fig. 10. Computed velocity profile in 70 t tundish at throughput rate of 4.1 t/min.

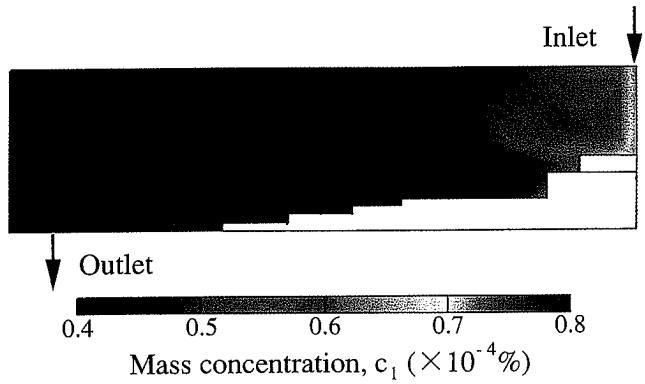

Fig. 11. Computed contours of cluster concentration (clustering degree: number of particles in cluster, $i=1$) in 70 t tundish at throughput rate of 4.1 t/min.

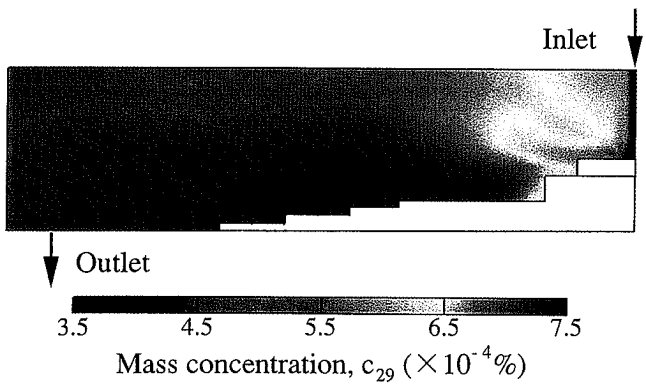

Fig. 12. Computed contours of cluster concentration (clustering degree: number of particles in cluster, $i=29$) in 70 t tundish at throughput rate of 4.1 t/min.

the other forming a surface current that follows the surface of the molten metal. At the side wall, this surface current forms a downward current, and either is discharged from the tundish through the immersion nozzle or returns to the center of the bottom and forms a large circulating counterflow in the vicinity of the pouring flow. Although not illustrated here, it might also be mentioned that the results of calculations using water as the fluid and the measured values of the velocity profile obtained with a water model showed good agreement. It can be conjectured that the results with molten steel would be substantially the same.

The computed concentration contours of alumina clusters with clustering degrees of 1 and 29 are shown in **Figs. 11** and **12**, respectively. It can be understood from these figures that, during the movement of the

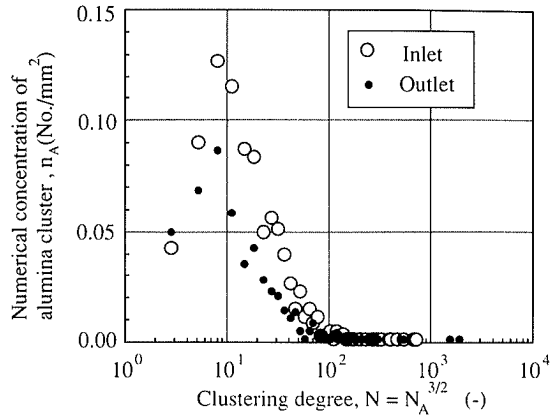

Fig. 13. Relationship between observed numerical concentrations of alumina clusters and clustering degree (number of particles in cluster).

cluster from the upper stream to the lower stream, the concentration of inclusions with a clustering degree of 1 decreases, whereas the concentration of inclusions with a clustering degree of 29 increases. These agglomerations are remarkable in the vicinity of the jet stream from the pouring pipe. Because the turbulent intensity of the flow is large in this area, the calculation results of the concentration of clusters are considerably influenced by Hamaker's constant which effects turbulent coagulation coefficient. Taniguchi *et al.* predicted that Hamaker's constant of alumina in liquid iron is 2.3×10^{-20} (J).[17] In this case, the coagulation coefficient is 1.48 times of the value used in this study.

4.2.2. Agglomeration Characteristics of Alumina Clusters

Figure 13 shows the concentration distribution of alumina clusters by clustering degree as obtained from bomb samples of molten steel in the tundish at the bottom of the inlet and the top of the outlet. The ordinate in this figure shows the numerical concentration of the alumina clusters, n_A, and the abscissa shows the clustering degree. Because measurements were made on a 2-dimensional plane, the clustering degree on the abscissa was adjusted using $N=N_A^{3/2}$ in order to convert the 2-dimensional measurements to three dimensions. The concentration of inclusions with clustering degrees of $N=5$ to approximately 90 decreased at the outlet. However, quantitative evaluation of inclusions with higher clustering degrees is difficult due to their low frequency of appearance.

Figure 14 shows the concentration distribution by clustering degree at the inlet and outlet as obtained by numerical calculation. This figure also shows the observed results of the numerical density in a plane from Fig. 13, converted here to mass concentration values. The calculated results showed good agreement with the observed results. It should be mentioned that the calculated distribution of the concentration of inclusions at the outlet reached its largest value at the maximum clustering degree because the effect of floating and separation was small due to the fact that the maximum clustering degree was set to a somewhat low value in the

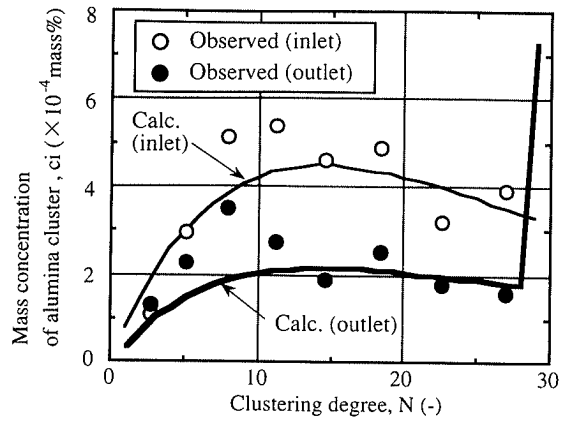

Fig. 14. Relationship between mass concentration of alumina clusters and clustering degree (number of particles in cluster).

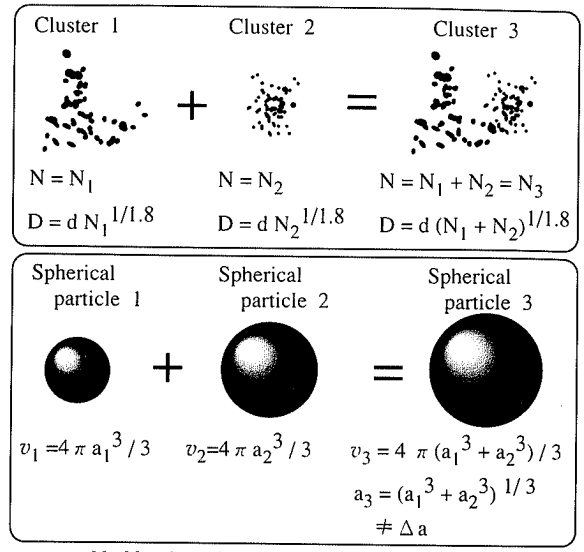

N : Number of particles in cluster
D : Diameter of cluster
d : Diameter of particles in cluster
v : Volume of spherical particle
a : Radius of spherical particle
Δa : Adjustment of radius for calculation

Fig. 15. Comparison of cluster model of agglomeration and spherical particle model.

calculation. If the calculations had been made considering higher clustering degrees, it is conceivable that the distribution would be smoother. Another influence of limitation of maximum clustering degree on calculation result is as follows. The collision and coalescence of clusters below 29 clustering degrees and over 29 clustering degrees is ignored. The concentration of 29 clustering degrees inclusions is overestimated because the effect of floating and separation was small in comparison with that of inclusions over 29 clustering degrees. Consequently it is considered that the result is not much influenced by the limitation of maximum clustering degree.

It can therefore be said that the agglomeration and floating separation of cluster inclusions in molten steel are simulated satisfactorily with this model.

4.2.3. Comparison of New and Conventional Computational Models

The computational model for alumina clusters using fractal theory is superior to the conventional model in the following points.

First, as shown in the upper part of **Fig. 15**, the fractal model shows the same mass before and after coalescence because cluster-shaped inclusions with N_1 and N_2 constituent particles coalesce to form an inclusion with $N_1+N_2=N_3$ constituent particles. On the other hand, the conventional models of agglomeration[3,4] are susceptible to rounding errors, as shown in the lower part of Fig. 15. Specifically, when spherical inclusions with radii a1 and a2 coalesce, the radius of the sphere after coalescence are generally not identical with the radius which is set for computational reasons in order to decide the radius of the sphere so that the volume (or mass) of the original spherical inclusions is preserved, and this results in a rounding error.

Second, as mentioned in Fig. 7, in this model, the floating velocity of large inclusions is smaller than in the conventional models, which provides an easier understanding of the large cluster inclusions that are occasionally seen in slabs.

Third, in the conventional models, when a small-radius particle (a_1) coalesces with a large-radius particle (a_2), there are cases in which the small-radius particle disappears computationally while the radius of the large-radius particle remains unchanged, which also gives rise to errors in the numerical density distribution. This problem occurs when the volume of the particle with radius a_1 is small in comparison with the difference between the volumes of the particle with radius a_2 and the particle with the next largest radius $(a_2+\Delta a)$. Conventionally, computational means are adopted to reduce these errors, for example, by maintaining the same total volume of the inclusions,[3] but it is not possible to eliminate the distortions in the numerical density distribution. With the new computational model, it is not necessary to consider the above-mentioned error. Thus, this model is capable of providing an accurate grasp of the behavior of cluster-shaped inclusions, and is expected to contribute to future research in this field.

5. Conclusion

The characteristics of alumina clusters in molten steel were quantified using fractal theory, and cold experiments were performed to investigate the floating behavior of clusters. The following results were obtained regarding the floating and agglomeration of alumina clusters in molten steel.

(1) The fractal dimension of alumina clusters in molten steel is 1.8.

(2) By introducing the fractal dimension, it is possible to derive the following equations for the floating velocity of cluster-shaped inclusions of 10 clustering degrees and over, which consider the changes in average density that accompany changes in the diameter of clusters.

$$v=\frac{8}{5}\frac{D^{0.8}d^{1.2}(\rho-\rho_p)g}{18\mu} \quad Re\leqq 3 \quad \text{.....(24)}$$

$$v=\frac{D^{0.2}d^{0.8}(\rho-\rho_p)^{2/3}g^{2/3}}{6^{2/3}\rho^{1/3}\mu^{1/3}} \quad 3<Re<100 \quad .....(25)$$

(3) In comparison with the conventional equations, which assume a constant average density, the dependency of the floating velocity on the cluster diameter is small in the equations obtained in (2). In particular, the floating velocity of clusters larger than 100 μm is considerably smaller than the floating velocity obtained with the conventional models.

(4) A model of the coalescence of cluster-shaped inclusions was constructed and applied to alumina clusters in molten steel in the tundish. The calculated results showed good agreement with the measured results, demonstrating that it is possible to simulate the agglomeration and floating separation of cluster inclusions using this model.

REFERENCES

1) U. Lindborg and K. Torssel: *Trans. Metall. Soc. AIME*, **242** (1968), 94.
2) S. Linder: *Scand. J. Metall.*, **3** (1974), 137.
3) K. Nakanishi and J. Szekely: *Trans. Iron Steel Inst. Jpn.*, **15** (1975), 522.
4) K. Shirabe and J. Szekely: *Trans. Iron Steel Inst. Jpn.*, **23** (1983), 465.
5) K. Asano and T. Nakano: *Tetsu-to-Hagané*, **57** (1971), 1943.
6) K. Okohira, N. Sato and H. Mori: *Tetsu-to-Hagané*, **59** (1973), 1166.
7) J. H. Perry: Chemical Engineers' Handbook, McGraw-Hill, New York, (1963), 5–59.
8) J. Feder: Fractals, Plenum, New York, (1988), 33.
9) S. Taniguchi and A.Kikuchi: *Tetsu-to-Hagané*, **78** (1992), 527.
10) M. Smoluchowski: *Z. Phys. Chem.*, **92** (1917), 129, 155.
11) K. Higashitani, K. Yamaguchi, Y. Matuno and G. Hosokawa: *J. Chem. Eng. Jpn.*, **16** (1983), 299.
12) P. G. Saffman and J. S. Turner: *J. Fluid. Mech.*, **1** (1956), 16.
13) B. E. Launder and D. B. Spalding: Lectures in Mathematical Models of Turbulence, Academic Press, London, (1972), 90–110.
14) R. T. DeHoff and F. N. Rhines: Quantitative Microscopy, McGraw-Hill, New York, (1968), 158.
15) R. Jullien, M. Kolb and R. Botet: *J. Phys. Lett.*, **45** (1984), L-211.
16) J. Happel and H. Brenner: Low Reynolds Number Hydrodynamics, Prentice-Hall, Englewood Cliffs, (1965), 249–270.
17) S. Taniguchi, A. Kikuchi, T. Ise and N. Shoji: *ISIJ Int.*, **36** (1996), S117.